Low temperature atomic-scale observations of slip traces in niobium

B. Douat, J. Bonneville, M. Drouet, Loranne Vernisse, C. Coupeau

▶ **To cite this version:**

B. Douat, J. Bonneville, M. Drouet, Loranne Vernisse, C. Coupeau. Low temperature atomic-scale observations of slip traces in niobium. Scripta Materialia, 2020, 183, pp.81 - 85. 10.1016/j.scriptamat.2020.03.026 . hal-03489958v1

HAL Id: hal-03489958

https://hal.science/hal-03489958v1

Submitted on 22 Aug 2022 (v1), last revised 16 Apr 2024 (v2)

HAL is a multi-disciplinary open access archive for the deposit and dissemination of scientific research documents, whether they are published or not. The documents may come from teaching and research institutions in France or abroad, or from public or private research centers.

L'archive ouverte pluridisciplinaire **HAL**, est destinée au dépôt et à la diffusion de documents scientifiques de niveau recherche, publiés ou non, émanant des établissements d'enseignement et de recherche français ou étrangers, des laboratoires publics ou privés.

Distributed under a Creative Commons Attribution - NonCommercial 4.0 International License

Version of Record: https://www.sciencedirect.com/science/article/pii/S1359646220301585
Manuscript_dcb526c0e8450c77147cf87ea25d0949

Low temperature atomic-scale observations of slip traces in niobium

B. Douat, J. Bonneville, M. Drouet, L. Vernisse, C. Coupeau*

Institut Pprime, Université de Poitiers/CNRS/ENSMA - UPR 3346,

SP2MI, Teleport 2, Bd. M. et P. Curie, F-86962 Chasseneuil-Futuroscope, France

Abstract. Slip traces in body-centred cubic single crystals usually correspond to various slip planes and even, in the case of wavy slip traces, to none identifiable crystallographic slip planes. We recently developed an experimental scanning tunnelling microscope that allows characterizing slip traces at the atomic scale. Unique experimental results obtained at 200 K and 293 K have already been published. We report here new relevant experimental results obtained at 90 K on niobium single crystals, that provide additional information in the understanding of the motion of screw dislocations in bcc metals.

Keywords: bcc metals, slip traces, dislocation, UHV-STM

*corresponding author: christophe.coupeau@univ-poitiers.fr

© 2020 published by Elsevier. This manuscript is made available under the CC BY NC user license
https://creativecommons.org/licenses/by-nc/4.0/

Although not all pure body-centred cubic (bcc) metals behave in the same way, mechanical tests early established that, mainly for temperatures below room temperature, their flow stress drastically increases at decreasing temperatures and could exhibit some violations to the Schmid's law, depending on both the orientation and the sign of the applied stress [1,2]. In addition, *post mortem* and *in situ* transmission electron microscope (TEM) observations performed in the low temperature regime showed that long screw dislocations were predominant in the microstructures [3,4]. These experimental results were supplemented by activation parameter measurements. Small activation volume values, of the order of a few b^3 (b is the magnitude of the Burgers vectors), were deduced from measurements of the strain rate sensitivity of the stress, indicating very localised thermally activated events [5-8]. In agreement with these activation volume values, associated activation enthalpies deduced either from tensile tests [5-8] or internal friction experiments [9,10] also suggested a highly local thermally activated process. All the above results constituted a body of proof that bcc plasticity was controlled by the nucleation and the migration of kink pairs along screw dislocations [2,11], which is still today a consensus in the field of materials science.

The thermally activated character of these elementary mechanisms implies an athermal temperature T_a above which they are no more rate controlling. The energy barrier associated with this latter mechanism is very sensitive to both the dislocation core structure and the kink height, which should normally lead to a restricted number of possible families of slip planes. However, slip traces left at sample surfaces by the motion of emerging dislocations may experimentally correspond to various slip planes such as {011}, {112}, {123} and even, in the case of wavy slip traces, to none identified crystallographic slip planes [2,12,13]. Investigations using, for instance, scanning electron microscopy [14], atomic force microscopy [15] or even sophisticated Laue diffraction technique on micro-pillars [16] cannot unfortunately give information on the dislocation propagation at the atomic scale. Recently, slip traces imaged at the atomic scale using a dedicated device, which combines a scanning tunnelling microscope (STM) stage coupled with a compression set-up under ultra-high vacuum (UHV), were reported [17]. These experiments were restricted to the temperature range $[T_c\text{-}T_a]$, that is, above the temperature T_c (~175 K for Nb) and below the athermal temperature T_a (~340 K for Nb). T_c is the lower limit of the temperature domain of occurrence of non-crystallographic glide, below which non-crystallographic slip progressively vanishes.

In this context, the present paper reports an experimental study of atomic scale resolved slip traces obtained on deformed Nb single crystals at a temperature below T_c. The samples

were deformed in compression at 90 K and surface observations were *in situ* performed using the Nanoplast device facilities [18]. The present slip trace observations are compared with previous STM investigations at 200 K and 293 K [17], in particular regarding the number and predominant associated crystallographic planes.

The experimental procedures have already been detailed elsewhere [17,18] and are here briefly recalled. Niobium single crystals of high purity (the main impurities are Ta, C and O with content of 180 ppm, 25 ppm and 15 ppm, respectively) were first mechanically polished under atmospheric conditions. The sample sizes are nearly 2 mm x 2 mm in cross section with a gauge length of 6 mm. For achieving atomic resolution, the samples were then cleaned under UHV environment, at a base pressure of about 10^{-10} mbar, by successive cycles of Ar^+ sputtering (1 kV at 6 µA, for 5 min) and annealing at 1275 K for 2 hours. The compression axis is along the $[\bar{1}12]$ crystallographic direction and the observation surface is $(1\bar{1}1)$ oriented (see Fig. 1). These geometrical conditions lead according to the literature to <111>{110} and <111>{112} as predominant slip systems. It must be emphasised that, using various possible slip-trace analysis procedures at the atomic scale, the {123} slip planes were also occasionally examined but not univocally detected, so that our analysis method presented hereafter does not account for such planes that have never been unambiguously evidenced experimentally in the low temperature deformation domain of Nb. The associated Schmid factors m are given in Table 1 for the a/2[111] Burgers vector, as well as the angles θ between the slip traces and the compression axis. Note that, for this symmetrical orientation, the a/2$[\bar{1}\bar{1}1]$ Burgers vector is also activated. The associated planes are the (011) and the $(\bar{1}21)$ planes; related slip traces lying at θ = -60° and θ = -71° have been experimentally observed, sometimes on a same STM scan area. However, as in [17] for the sake of clarity, only the results regarding the former Burgers vector are presented. Shears that would occur in the twinning (Tw) and anti-twinning (ATw) senses are also distinguished in the following.

Typical slip traces (white lines) obtained at 90 K under stress (τ ~ -235 MPa) by STM for a plastic strain γ_p = -2.7% on the Nb$(1\bar{1}1)$ surface are shown in Fig. 2a. Surface profiles randomly extracted perpendicularly to the slip traces (see Fig. 2b for a characteristic profile) indicate that each slip trace was produced by the motion of a single emerging dislocation, *i.e.* the experimental slip trace height of approximately 100 pm is in fair agreement with the projection of the a/2[111] Burgers vector onto the normal of the $(1\bar{1}1)$ imaging surface given by $h = \vec{n}.\vec{b} = \frac{a}{2\sqrt{3}}$ = 95 pm, for a lattice parameter a = 0.33 nm. STM images reveal that the

Nb{111} surface exhibits a (2x2) reconstruction, as previously reported in the literature [19].

Close inspection reveals that the slip traces consist of a succession of nanometric segments of different orientations and lengths containing periodic sequences of atomic steps. The intersections of the $(1\bar{1}1)$ observation surface plane with the {110} and {112} planes are schematized in Fig. 3. Due to the crystallographic nature of the surface, each slip trace is composed of atomic steps lying along the two [110] and [011] dense atomic rows. The analysis procedure consists of slicing the slip traces in segments of i atomic steps using a random or a pertinent origin on the slip trace. The local angles θ_i of the segments with respect to the compression axis are then measured all along each trace to finally extract an angular distribution. The purpose is now to determine the value of i for which it exists a unique relation between the angular distribution N=f(θ_i) and the associated planes considered in this work. The theoretical angular distributions for the five associated planes are presented in Fig. 3 at increasing i values.

For instance, let us consider the case of a slip trace at $\theta = 60°$. The related theoretical angular distributions are presented in Fig. 3c for $i \in [1;6]$. For i=1, the trace signature is an angular distribution composed of two peaks, one at $\theta_1 = 30°$ and the other one at $\theta_1 = 90°$, whose proportions are 1/2 and 1/2, respectively. Unfortunately, each peak also corresponds to either the $(0\bar{1}1)$ or the $(\bar{1}10)$ plane (see Fig. 3a and e). Thus, the identification of the actual associated plane is consequently not possible for i=1. The angular distribution for i=2 is composed of a single peak at $\theta_2 = 60°$. Similar sequences are obtained for higher i values. Note that starting the analysis at another atomic position along the trace will lead to the same theoretical angular distribution.

Considering the other angular distributions in Fig. 3, the slip traces and their associated crystallographic planes that can be identifiable (*i.e.* only one peak on the angular distribution as described previously for a trace at $\theta = 60°$) are reported in Fig. 4, for increasing i values. It is seen that it is necessary to go up to i = 6 in order to unambiguously identify the five considered planes. Therefore, the minimum number i of atomic steps that must be considered for our analysis corresponds to the least common multiple of 1, 2 and 3, which is 6. Hereafter, a segment of six atomic surface steps, *i.e.* i=6, is referred to as a standard segment, which has been used for slicing each slip trace. It has been verified that choosing a random or a pertinent origin for the standard segment was not significantly modifying the set of θ_6 angles obtained along a given slip trace resulting from various planes. Consequently, the path of screw dislocations was extracted from our analysis procedure between two atomic positions along

the single traces, that are distant by a maximum length of the standard segment, given by $6\times2\sqrt{2}a$ owing to the Nb (2x2) surface reconstruction [19]. For Nb, it corresponds to 5.6 nm.

Fig. 5 shows how the proportions of standard segments are distributed into each type of planes. The analysis was carried out on 13 slip traces of various lengths (ranging from 13 to 78 nm). It should be noted that a total length of 566 nm of single slip traces has been investigated, which may seem rather modest but corresponds to several hundreds of high-resolution STM images. Fig. 5 clearly indicates that, at 90 K, slip traces are associated with $(\bar{1}01)$ and $(\bar{2}11)^{Tw}$ planes only. All slip traces are composed of segments that belong to these two planes, except for one slip trace (the shortest of 13 nm length) that is associated with a $(\bar{1}01)$ plane only. Therefore, in our experimental conditions of stress state at 90 K, as at 200 K and 293 K [17], the observation of $(\bar{1}01)$ associated plane indicates that screw dislocations in bcc metals may have in Peierls valley a compact core configuration similar to that of the predictions of density functional theory (DFT) calculations at zero stress [20, 21], because only this core configuration may yield slip traces associated with $(\bar{1}01)$ plane. The $(0\bar{1}1)$ and $(\bar{1}10)$ slip planes, with low Schmid factors (see Table 1), are not detected. Furthermore, slip traces associated with $(11\bar{2})^{ATw}$ planes are not evidenced, that is, anti-twinning shear is not activated below T_c, in agreement with the literature [2]. The lack of slip traces associated with the $(0\bar{1}1)$ and $(\bar{1}10)$ planes does not imply that kink pairs are not nucleated on these planes. Indeed, according to DFT calculations, slip onto {112} planes can only result from a composition of elementary atomic displacements, *i.e.* kink pairs, onto {011} slip planes [20,21]. Decomposing the $(\bar{2}11)^{Tw}$ contribution as an equal mixture of the two {011} planes leads to a proportion of nearly 73 % for the $(\bar{1}01)$ plane and 27 % for the $(\bar{1}10)$ plane. The lack of evidence of the $(0\bar{1}1)$ planes strongly suggest that, at 90 K, kink pairs are always produced on $(\bar{1}10)$ planes, which when associated with $(\bar{1}01)$ kink pairs lead to the $(\bar{2}11)^{Tw}$ slip traces. This result may be interpreted in the frame of the work of Dezerald *et al.* [22] who have determined by *ab initio* atomistic simulations that the displacement of a screw dislocation from a <111> dense atomic row to the next one onto {110} planes are not rectilinear but follow curled trajectories that would greatly enhance dislocation motion onto $(\bar{1}10)$ planes to the detriment of $(0\bar{1}1)$ planes. In this case, they proposed that the usual Schmid factors must be replaced by more adequate orientation factors given in Table 1. These corrected Schmid factors m^* make clear the lack of $(0\bar{1}1)$ elementary slip and the reinforcement of $(\bar{1}10)$ elementary slip with respect to the primary $(\bar{1}01)$ planes. A support to these latter theoretical predictions has been recently given in a study using DFT calculations

coupled with the nudged elastic band (NEB) method showing that such a curled trajectory of the screw dislocation core in W is in fact associated with an elliptical and tilted core deformation [23].

A similar decomposition of the results obtained at 200 K in [17] gives 76 % for the $(\bar{1}01)$ planes, 15 % for the $(\bar{1}10)$ and 9 % for the $(0\bar{1}1)$ planes. The proportions of $(\bar{1}01)$ slip are almost similar at 90 K and 200 K, but the occurrence of $(\bar{1}10)$ elementary is observed at 200 K. This may be due to a stress effect (*i.e.* at high temperature, the applied stress is lower) and to the contribution of thermal activation, which is higher at 200 K.

To summarize, *in situ* UHV-STM imaging of slip traces at sample free surface of Nb single crystals deformed in compression tests performed at 90 K have been reported. The experimental results share some similarities with those already obtained in a previous study at 200 K and 293 K. In particular, each slip trace results from the emergence of single dislocations. Because dislocation sources are expected to emit more than a single dislocation, this result can be attributed to the ease of cross slip of the screw dislocations in bcc crystals. None of the slip traces can be associated with the $(0\bar{1}1)$ and $(\bar{1}10)$ slip planes, but all slip traces exhibit crystallographic segments that belong to the $(\bar{1}01)$ planes. The latter result would be in agreement with DFT calculations predicting a compact core of the screw dislocations involved in plasticity in bcc materials. When compared with the results at higher temperatures, a major difference appears in the crystallographic planes that can be associated with the slip traces. It is shown that, at the atomic scale, the slip traces are composed of crystallographic segments that at 90 K can be only associated with $(\bar{1}01)$ and $(\bar{2}11)^{Tw}$ planes, whereas $(11\bar{2})^{ATw}$ planes were also observed at 200 K and 293 K.

Acknowledgments. This work was supported by the French Government Program "Investissements d'Avenir" (LABEX INTER-ACTIFS, reference ANR-11-LABX-0017-01) and was financially supported by the "Region Poitou-Charentes". Dr Ladislas Kubin is greatfully acknowledged for fruitful discussions.

References

[1] J.W. Christian, Metall. Trans. A 14 (1983) 1237-1256.

[2] C.R. Weinberger, B.L. Boyce, C.C. Battaile, Int. Mater. Rev. 58 (2013) 296-314.

[3] A. Lawley, H.L. Gaigher, Philos. Mag. 10 (1964) 15-33.

[4] F. Louchet, L.P. Kubin, D. Vesely, Philos. Mag. A 39 (1979) 433-454.

[5] G. Sargent, Acta Metall. 13 (1965) 663-671.

[6] J.D. Meakin, Can. J. Phys. 45 (1967) 1121-1134.

[7] P. Groh, R. Conte, R. Acta Metall. 19 (1971) 895–902.

[8] L.P. Kubin, B. Jouffrey, Philos. Mag. 27 (1973) 1369-1385.

[9] F. De Lima, W. Benoit, Physica Status Solidi a 67 (1981) 565-572.

[10] G. D'Anna, W. Benoit, Materials Science and Engineering: A 164 (1993) 191-195.

[11] A. Seeger, U. Holzwarth, Philos. Mag. 86 (2006) 3861-3892.

[12] H. Matsui, H. Kimura, H. Saka, K. Noda, T. Imura, Mater. Sci. Eng. 53 (1982) 263-272.

[13] G. Taylor, J.W. Christian, Philos. Mag. 15 (1967) 873-892.

[14] P. Franciosi, L. Le, G. Monnet, C. Kahloun, M.-H. Chavanne, Int. J. Plast. 65 (2015) 226-249.

[15] D. Charrier, J. Bonneville, C. Coupeau, Y. Nahas, Scr. Mater. 66 (2012) 475-478.

[16] C. Marichal, H. Van Swygenhoven, S. Van Petegem, C. Borca, Sci. Rep. 3 (2013) 2547.

[17] B. Douat, C. Coupeau, J. Bonneville, M. Drouet, L. Vernisse, L.P. Kubin, Scr. Mater.162 (2019) 292-295.

[18] Y. Nahas, F. Berneau, J. Bonneville, C. Coupeau, M. Drouet, B. Lamongie, M. Marteau, J. Michel, P. Tanguy, C. Tromas, Rev. Sci. Instrum. 84 (2013) 105117.

[19] C. Coupeau, J. Durinck, M. Drouet, B. Douat, J. Bonneville, J. Colin, J. Grilhé, Surf. Sci. 632 (2015) 60–63.

[20] S.L. Frederiksen, K.W. Jacobsen, Philos. Mag. 83 (2003) 365-375.

[21] D. Rodney, L. Ventelon, E. Clouet, L. Pizzagalli, F. Willaime, Acta Mater. 124 (2017) 633-659.

[22] L Dezerald, D. Rodney, E. Clouet, L. Ventelon, Nat. Commun. 7 (2016) 11695.

[23] A. Kraych, E. Clouet, L. Dezerald, L. Ventelon, F. Willaime, D. Rodney, Computational Materials 5 (2019) 109.

Figure captions

Figure 1. Schematic representation of the Nb samples showing the orientations of the $(1\bar{1}1)$ surface and $[\bar{1}12]$ compression axis. A slip trace left by a moving dislocation with Burgers vector $\vec{b}$ is characterized by its angle θ with the compression axis.

Figure 2. (a) Typical atomic-scale STM image at 90 K. The slip traces are seen with a white contrast on the $(1\bar{1}1)$ observation surface. The resolved shear stress and plastic strain are respectively τ = -235 MPa and γ_p = -2.7%. (b) Characteristic profile perpendicular to the slip traces. The height *h* of each slip trace is approximately 100 pm, corresponding to the passage of a single dislocation.

Figure 3. Theoretical angular distributions for $i \in [1;6]$ and for the (a) $(0\bar{1}1)$, (b) $(11\bar{2})^{ATw}$, (c) $(\bar{1}01)$, (d) $(\bar{2}11)^{Tw}$ and (e) $(\bar{1}10)$ associated planes.

Figure 4. Sets of identifiable associated planes along a slip trace, with respect to the number of atomic slip steps *i* of the standard segment used for the analysis.

Figure 5. Distribution of associated planes at 90 K for the 13 slip traces. Each of them is associated with a single color. The horizontal lines correspond to the mean values of the proportion of associated planes.

Table caption

Table 1: θ angle between the slip trace and the compression axis, Schmid factor m and corrected Schmid factor m^* from [22], for different slip planes related to the a/2[111] Burgers vector.

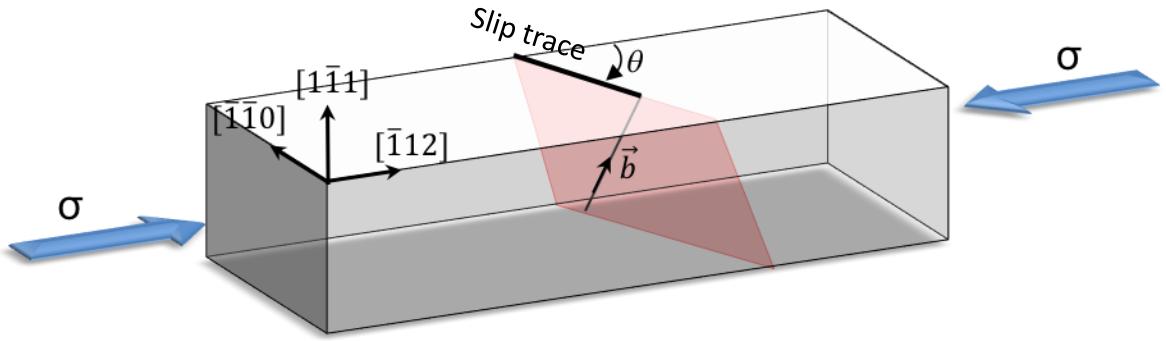

Figure 1. Schematic representation of the Nb samples showing the orientations of the $(1\bar{1}1)$ surface and $[\bar{1}12]$ compression axis. A slip trace left by a moving dislocations with Burgers vector $\vec{b}$ is characterized by its angle θ with the compression axis.

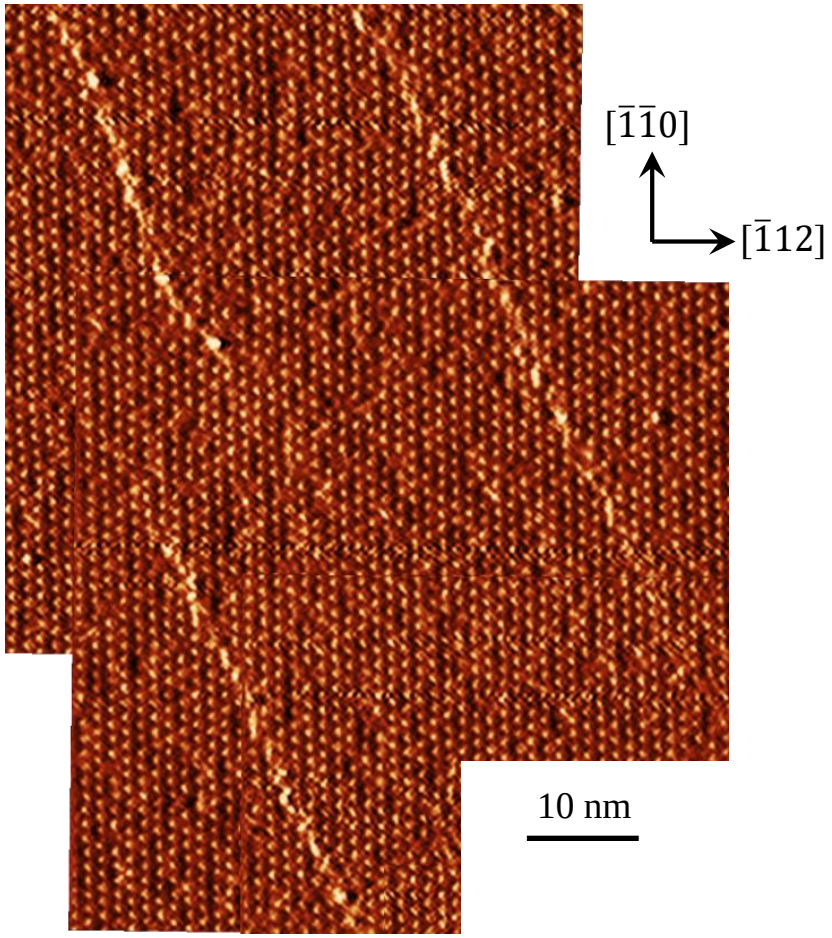

(a)

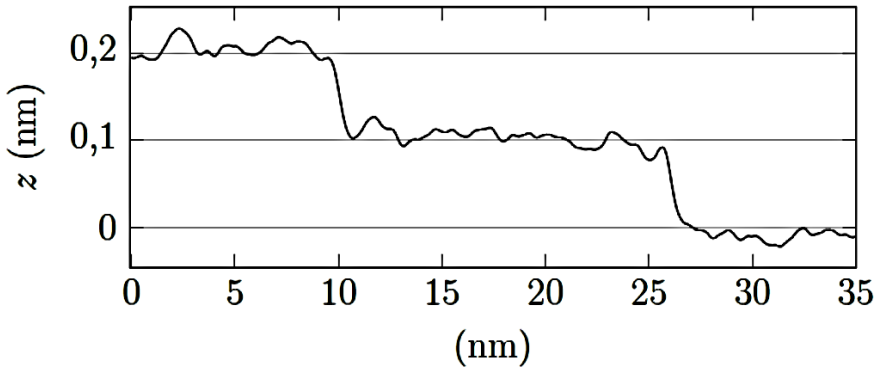

(b)

Figure 2. (a) Typical atomic-scale STM image at 90 K. The slip traces are seen with a white contrast on the ($1\bar{1}1$) observation surface. The resolved shear stress and plastic strain are respectively τ = -235 MPa and γ_p = -2.7%. (b) Characteristic profile perpendicular to slip traces. The height *h* of each slip trace is approximately equal to 100 pm, corresponding to the passage of a single dislocation.

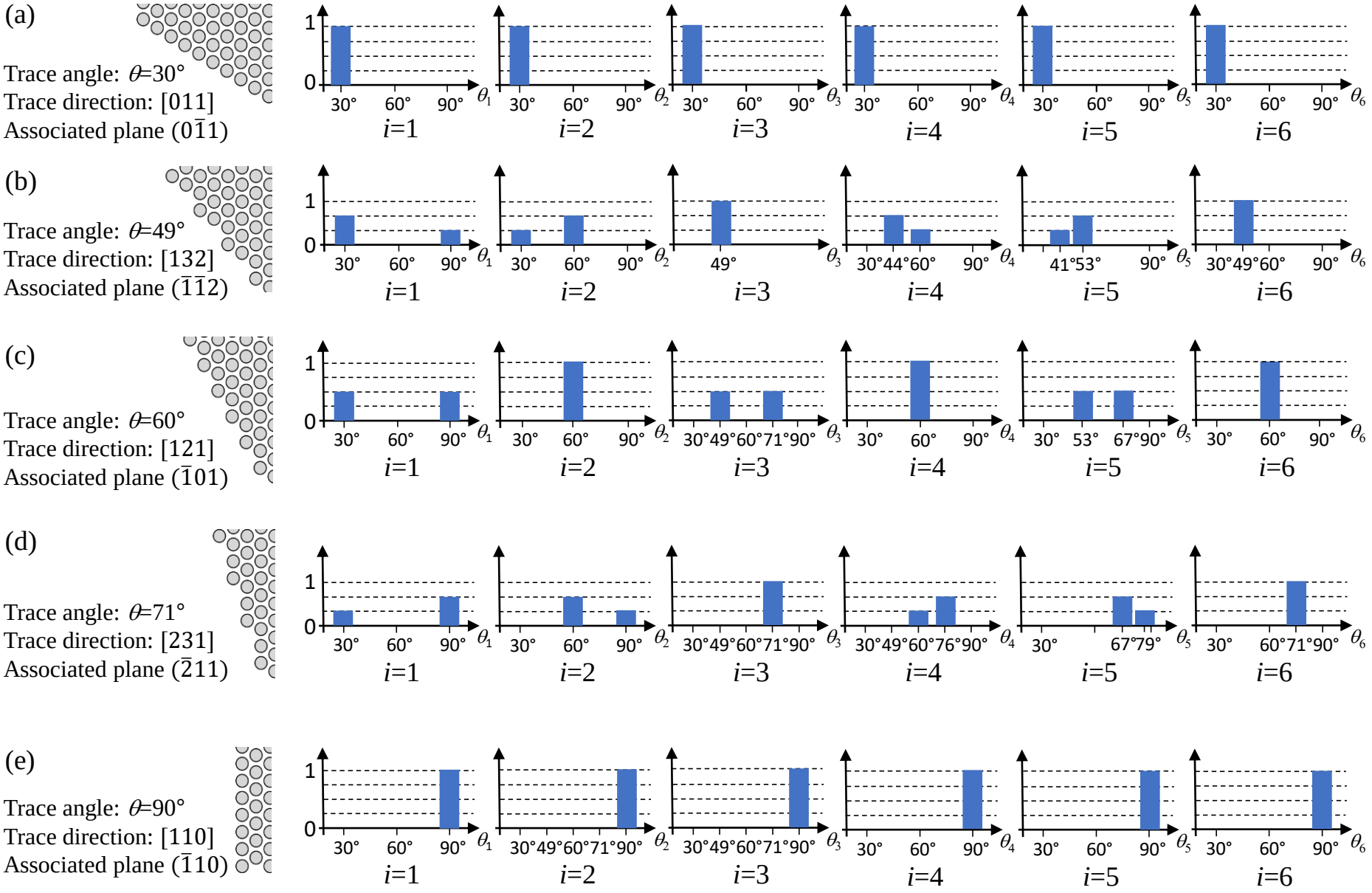

Figure 3. Theoretical angular distributions for $i \in [1;6]$ and for the (a) (0$\bar{1}$1), (b) ($\bar{1}\bar{1}$2), (c) ($\bar{1}$01), (d) ($\bar{2}$11) and (e) ($\bar{1}$10) associated planes.

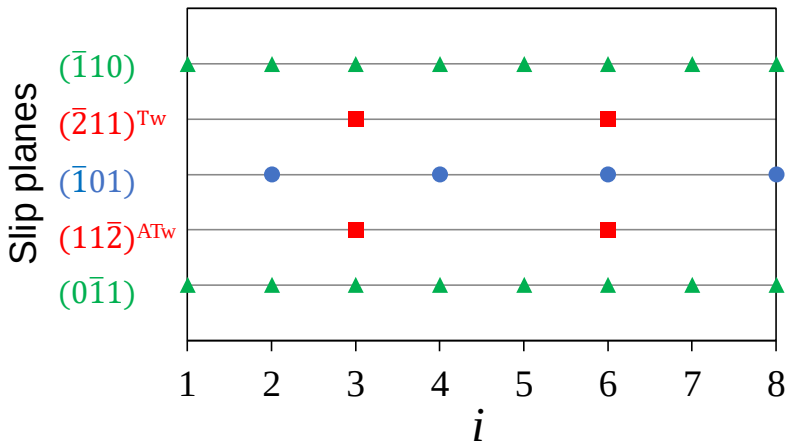

Figure 4. Sets of identifiable associated planes along a trace, with respect to the length *i* of the standard segment used for the analysis.

.

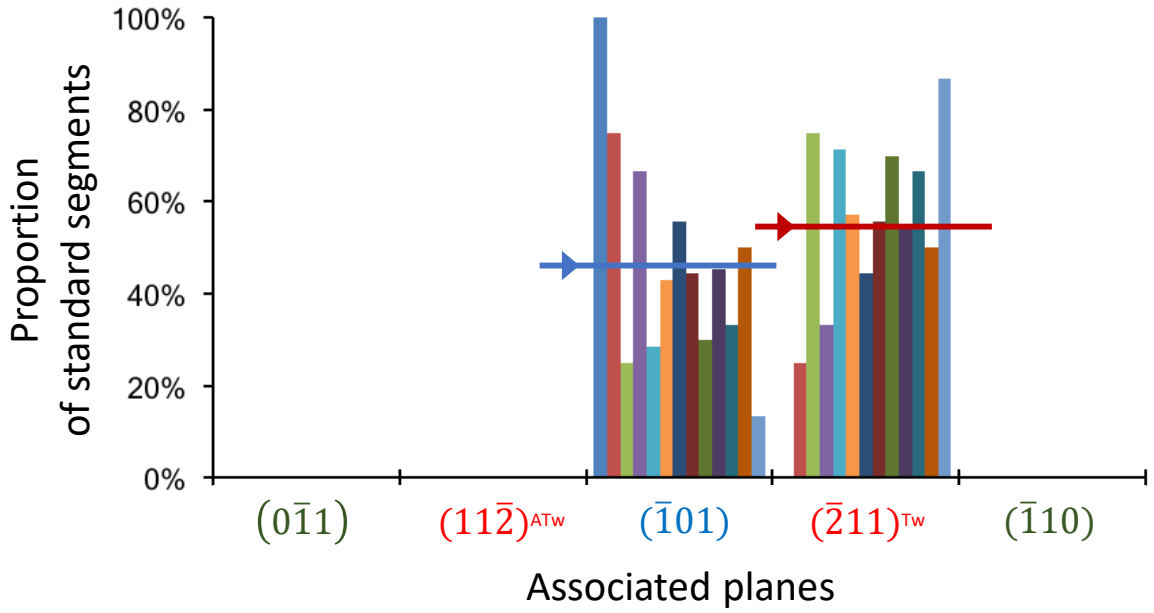

Figure 5. Distribution of associated planes at 90 K for the 13 slip traces. Each of them is associated with a single color. The horizontal lines correspond to the mean values of the proportion of associated planes.

Burgers vector b	Plane	Angle θ between slip trace and compression axis	Schmid factor m	Corrected Schmid factor m* [20]
½ [111]	$(\bar{1}01)$	60°	0.41	0.41
	$(\bar{2}11)^{Tw}$	71°	-	-
	$(11\bar{2})^{ATw}$	49°	-	-
	$(\bar{1}10)$	90°	0.27	0.37
	$(0\bar{1}1)$	30°	0.14	-0.02

Table 1: θ angle between the slip trace and the compression axis, Schmid factor m and corrected Schmid factor m* from [22], for different slip planes related to the a/2[111] Burgers vector.

Real dislocation movements in bcc single crystal revealed by atomic scale slip trace observations

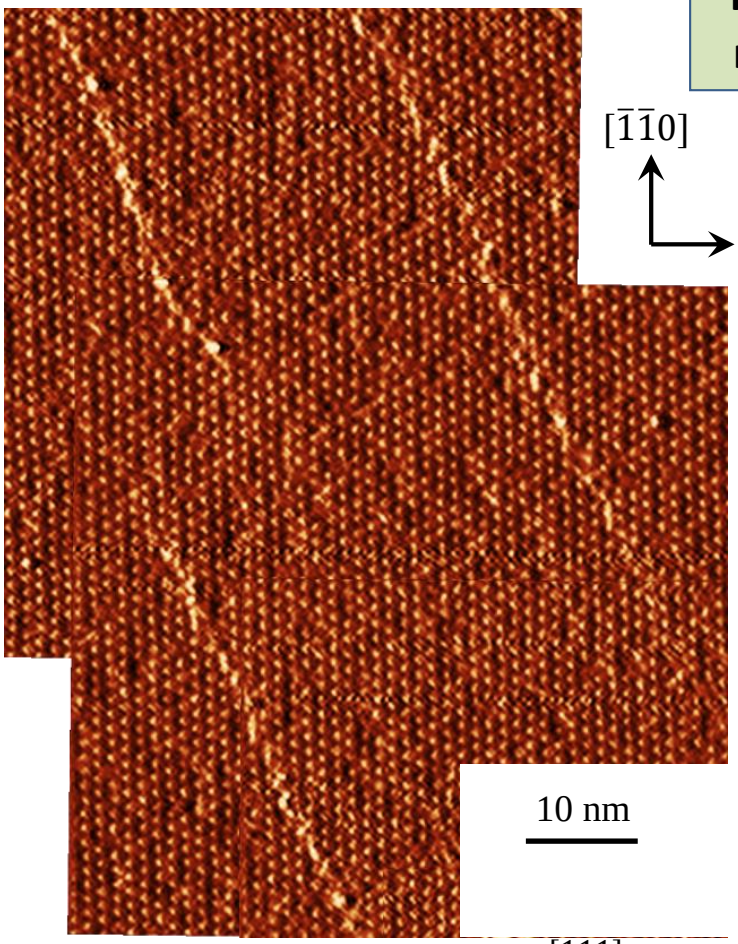

STM image of Nb single crystal surface strained at 90 K

Statistical analysis of the planes associated with dislocation slip traces